How to cite: Angew. Chem. Int. Ed. 2024, e202318559
doi.org/10.1002/anie.202318559

Metal-Organic Frameworks Hot Paper

Ultrastrong Electron-Phonon Coupling in Uranium-Organic Frameworks Leading to Inverse Luminescence Temperature Dependence

Dong-Hui Chen, Nina Vankova, Gautam Jha, Xiaojuan Yu, Yuemin Wang, Ling Lin, Frank Kirschhöfer, Raphael Greifenstein, Engelbert Redel, Thomas Heine, and Christof Wöll**

Abstract: Electron-phonon interactions, crucial in condensed matter, are rarely seen in Metal–Organic Frameworks (MOFs). Detecting these interactions typically involves analyzing luminescence in lanthanide- or actinide-based compounds. Prior studies on Ln- and Ac-based MOFs at high temperatures revealed additional peaks, but these were too faint for thorough analysis. In our research, we fabricated a high-quality, crystalline uranium-based MOF (KIT-U-1) thin film using a layer-by-layer method. Under UV light, this film showed two distinct "hot bands," indicating a strong electron-phonon interaction. At 77 K, these bands were absent, but at 300 K, a new emission band appeared with half the intensity of the main luminescence. Surprisingly, a second hot band emerged above 320 K, deviating from previous findings in rare-earth compounds. We conducted a detailed ab-initio analysis employing time-dependent density functional theory to understand this unusual behaviour and to identify the lattice vibration responsible for the strong electron-phonon coupling. The KIT-U-1 film's hot-band emission was then utilized to create a highly sensitive, single-compound optical thermometer. This underscores the potential of high-quality MOF thin films in exploiting the unique luminescence of lanthanides and actinides for advanced applications.

Introduction

As interest in the optoelectronic applications of metal–organic frameworks (MOFs) surges, understanding the fundamental properties of these often optically highly active crystalline materials becomes increasingly crucial.[1] While extensive research has been conducted on their optical absorption,[2] luminescence,[3] exciton transport,[4] and non-linear properties,[5] the study of electron-phonon coupling has remained relatively limited. Investigations into non-radiative decay and emission line broadening have been thorough; however, distinctly separated features like hot bands have rarely been discussed in case of MOFs. These hot bands manifest when radiative light emission is directly coupled with the relaxation of lattice vibrations. Although hot bands have been observed in MOFs, their low intensity in previous research has hindered an accurate identification of the underlying energetics and mechanisms.[6] This lack of understanding consequently limits the broader application of MOFs in optoelectronics. Notably, MOFs are much softer than conventional solids used in optoelectronics, like GaAs and perovskites, thus substantially decreasing their phonon energies.[7] Therefore, electron-phonon interactions in MOFs are expected to differ significantly from those in traditional inorganic solids and obtaining further information on this topic is urgently needed.

In this paper, we offer an in-depth luminescence analysis of uranium-based organic frameworks. Actinides are particularly well-suited for such research due to their complex electronic excitations.[8] Unlike the 4f states of lanthanides, the 5f states of actinides are less shielded, making them ideal

[*] Dr. D.-H. Chen, Dr. X. Yu, Dr. Y. Wang, F. Kirschhöfer, Dr. R. Greifenstein, PD Dr. E. Redel, Prof. Dr. C. Wöll
Institute of Functional Interfaces (IFG),
Karlsruhe Institute of Technology (KIT),
76344 Eggenstein-Leopoldshafen, Germany
E-mail: donghui.chen@kit.edu
christof.woell@kit.edu

Dr. N. Vankova, G. Jha, Prof. Dr. T. Heine
Fakultät für Chemie und Lebensmittelchemie,
TU Dresden,
Bergstraße 66c, 01069 Dresden, Germany

G. Jha, Prof. Dr. T. Heine
Helmholtz-Zentrum Dresden-Rossendorf,
Institut für Ressourcenökologie,
Bautzner Landstraße 400, 01328 Dresden, Germany

Dr. L. Lin
Institute of Nanotechnology
Karlsruhe Institute of Technology (KIT),
76344 Eggenstein-Leopoldshafen, Germany

Prof. Dr. T. Heine
Forschungsstelle Leipzig,
Helmholtz-Zentrum Dresden-Rossendorf,
Permoserstraße 15, 04318 Leipzig, Germany

candidates for studying the electron-phonon coupling between f-f transitions and vibrations of the metal–organic framework.[9] Although some indirect evidence of this coupling has been found in amorphous materials,[10] crystalline substances offer a more precise platform for spectroscopic research by minimizing inhomogeneous broadening.

Herein, we introduce a novel surface-mounted uranyl-based MOF thin film, $[UO_2(BTC)\cdot(HN(C_2H_5)_3)]_n$ (KIT-U-1), prepared by liquid-phase epitaxy (LPE) in a layer-by-layer (LbL) fashion. The LbL approach allowed for oriented growth tuning the thickness by adjusting the number of deposition cycles. The uranyl units in this MOF structure show a highly symmetric coordination to carboxylate groups, a situation favorable for strong electron-phonon coupling. Indeed, an extremely strong "hot band" emission was observed at higher temperatures, with an intensity of about 50 % of the direct luminescence bands. At low temperatures (77 K), this feature disappeared. Meanwhile, the other emission observed in the luminescence spectra exhibited the normal, opposite behavior: their intensity decreased with temperature. Furthermore, unexpectedly a second "hot-band" emission was observed upon heating to 320 K. In a final step, we demonstrated that the KIT-U-1 thin film can be used as a single-metal ratiometric luminescent thermometer with stable-wavelength, narrow emission bands. In conventional approaches, trivalent lanthanide-doped materials containing at least two different metals are used for the fabrication of ratiometric luminescent thermometers. However, unwanted energy transfer between different lanthanide ions can lead to significant discrepancies in the thermal behaviors of different production runs.[11]

The single-metal KIT-U-1 thin film presented here allows to overcome the inherent limitations of conventional bimetallic lanthanide materials, which have hindered their academic-to-industrial application. The intense "hot-band" emission phenomenon reported here for the KIT-U-1 thin films allowed to determine temperatures directly without the necessity for device-dependent calibration procedures. The KIT-U-1 thin film can achieve ratiometric thermal luminescence through the utilization of its unique physical emission properties, without the need for additional metal ions.

Results and Discussion

The KIT-U-1 thin films were prepared by liquid-phase epitaxy in an LbL fashion, as shown in Figure 1a.[12] In brief, a substrate with the functionalized surface was alternately immersed into the ethanolic solution of $UO_2(CH_2COO)_2\cdot 2H_2O$. and 1,3,5-Benzenetricarboxylic acid (BTC) using the LbL technique. A small amount of triethylamine (1.4×10^{-4} mol per liter) was added as a growth modulator. The deposition was carried out at a slightly elevated temperatures (50 °C) and normal atmospheric pressure. Continuous and homogeneous uranyl-MOF thin films, $[UO_2(BTC)\cdot(HN(C_2H_5)_3)]_n$, were fabricated on functionalized substrates with a thickness determined by the number of LbL cycles. Attempts to grow without growth modulator were not successful.

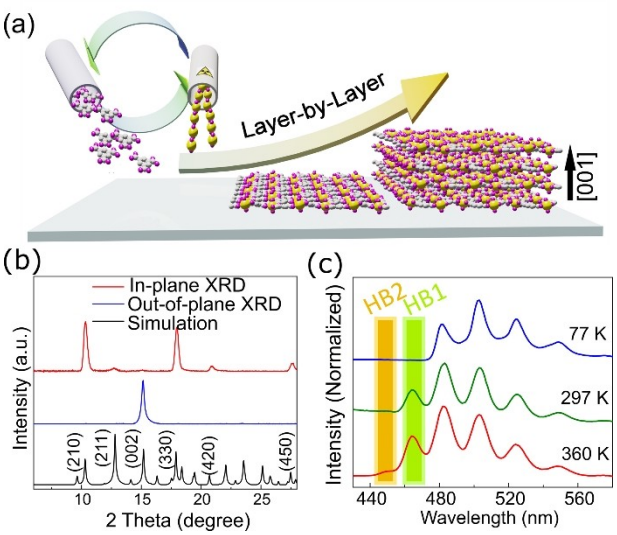

Figure 1. (a) Scheme of layer-by-layer assemble of KIT-U-1 thin film; (b) Out-of-plane, in-plane and simulated XRD patterns of the KIT-U-1 thin film; (c) Emission spectra of KIT-U-1 thin film at 77 K (blue), 297 K (green), and 360 K (red).

The in-plane and out-of-plane XRD-data (Figure 1b) show the presence of a well-ordered, highly oriented MOF thin film. Comparison to previously reported U-based MOFs revealed that this structure has not been reported before.[6c,13] Therefore, the structure of the KIT-U-1 was determined through a combination of experimental structure characterizations and density functional theory (DFT) calculations. In the proposed structure, negatively charged uranyl carboxylates, $[UO_2(RCOO)_3]^-$ units, are interconnected with six oxygen atoms of BTC linkers in the equatorial plane, thus forming a two-dimensional (2D) hexagonal layer.[14] The 2D layers are stacked in an ABAB stacking sequence along the [001] crystallographic direction. Protonated triethylamine ($[H\text{-}TEA]^+$) molecules are embedded into the pores of the hexagonal layer as positively charged guest molecules. Topologically, the uranyl units and the BTC ligands can be considered as 3-connected nodes, and the structure can be simplified as hexagonal planar net of hbc topology, as shown in Figure S2.[15]

The orientated nature of the KIT-U-1 thin film was evident from in-plane and out-of-plane X-ray diffraction (XRD) (Figure 1). A sharp peak from the (002) plane, which is oriented parallel to the surface, is clearly seen in the out-of-plane XRD pattern. Meanwhile, the in-plane XRD data revealed the diffraction peaks of (210), (211), (330), (420), and (450) planes. In-plane and out-of-plane X-ray diffraction demonstrated the oriented growth of the KIT-U-1 thin film in the LbL assembly. The 2D hexagonal layers were deposited parallel to the functionalized surface of the substrate. Since the number of diffraction peaks obtained in the out-of-plane and in-plane geometries was fairly small, the 2D KIT-U-1 thin films were also deposited on carboxyl-functionalized magnetic particles using a previously reported

LbL strategy.[16] For the particles, standard powder diffractograms could be recorded, which provided a substantially larger number of diffraction peaks than just the thin film in-plane and out-of-plane data. As shown in Figure S3, the XRD pattern of KIT-U-1 on magnetic particles is in excellent agreement with the simulated pattern, affirming the high accuracy of the resulting structure. The good stability of KIT-U-1 thin film was further demonstrated by temperature-dependent XRD, as illustrated in Figure S4.

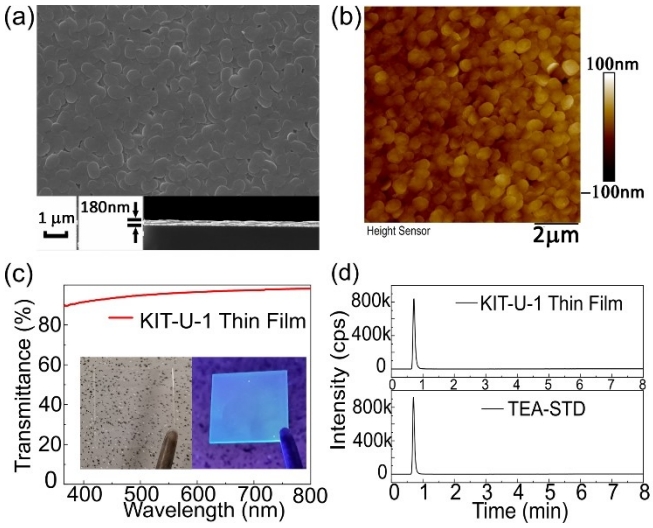

Figure 2. (a) SEM image of KIT-U-1 from a top view (top) and cross section (bottom); (b) AFM image of KIT-U-1; (c) UV–visible transmittance spectra of KIT-U-1 thin film in visible light range, inset: photographs of KIT-U-1 under sunlight (left) and 285 nm ultraviolet light (right); (d) Ultra performance liquid chromatography spectra from (top) KIT-U-1 and (bottom) 500 ng/ml standard solution of $[H\text{-}TEA]^+$ detected at m/z = +102.12 by LC-ESI-MS.

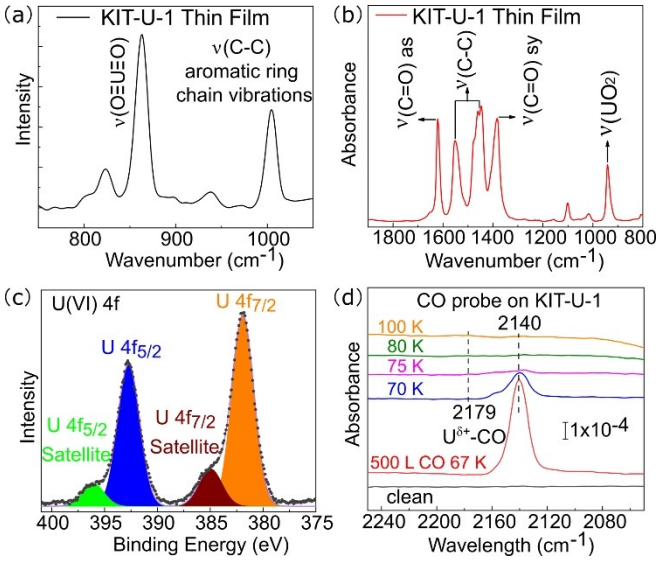

Figure 3. (a) Raman spectrum of KIT-U-1 thin film; (b) IRRAS spectrum of KIT-U-1 thin film; (c) XPS analysis of U 4f peaks in KIT-U-1 thin film; (d) Temperature-dependent UHV-FTIR spectra of CO desorption from KIT-U-1 thin film after preheating at 370 K for 20 min.

By utilizing the LbL growth method, continuous KIT-U-1 thin films can be produced on the surface with precise control over their thickness and roughness. The uniform surface coverage of KIT-U-1 thin film was demonstrated by scanning electron microscope (SEM) and atomic force microscope (AFM) images, see Figure 2. Undesired light scattering effects in the KIT-U-1 thin films were drastically reduced, thereby enabling the attainment of over 90 % transmittances in the visible light range.

The Raman and infrared reflection absorption spectra (IRRAS) are fully consistent with the proposed structure for the KIT-U-1. As shown in Figure 3, the symmetric stretch of $\nu(O\text{–}U\text{–}O)_{sym}$ is represented in the Raman spectrum as a strong peak at 863 cm^{-1}, indicating that uranyl ions are separated by organic linkers, without direct cation-cation interactions between uranyl units.[17] The corresponding asymmetric stretch of $\nu(O\text{–}U\text{–}O)_{asym}$ is observed in the IRRAS data at 947 cm^{-1}.[14b] Meanwhile, the frequencies of the asymmetric and symmetric stretch of the COO-groups between 1383–1618 cm^{-1} confirmed the complete coordination of carboxylates from the organic linker to the uranium atoms.[18]

In order to fully determine the structure of this previously unknown MOF type the possibility of the presence of guest molecules inside the MOF pores was investigated. Indeed, the presence of $[H\text{-}TEA]^+$, which was added as a growth modulator, was demonstrated in the KIT-U-1 thin film by Liquid Chromatography-Electrospray Ionization-Mass Spectrometry (LC-ESI-MS). A positively charged compound was detected at m/z = +102.12, which was consistent with the characteristics of $[H\text{-}TEA]^+$. The compound was demonstrated as $[H\text{-}TEA]^+$ by comparing it with a 500 ng/ml standard solution of $[H\text{-}TEA]^+$ using hyphenated high-performance liquid chromatography, as shown in Figure 2d (top). Meanwhile, the similar intensities of the dissolved solution and the standard solution in Figure 2d (bottom) indicated a high degree of consistency between the results of LC-ESI-MS and the 2D hexagonal layer structure of KIT-U-1 Emission spectra of KIT-U-1 thin film in 77 K (blue) and 297 K (red).

To gain further information on the possibility of free coordination sites at the uranyl units in the KIT-U-1 thin film, CO molecules were used as probe molecules. To this end, samples were introduced into an ultra-high-vacuum Fourier-transform infrared spectroscopy (UHV-FTIR) system with a base pressure of 1×10^{-10} mbar.[19] After a slight annealing at 370 K for 20 min the sample was cooled to 67 K using liquid Helium and then exposed to CO. UHV-FTIR spectra recorded after CO adsorption did not show any CO vibrational bands indicative of CO-$U^{\delta+}$ species, see Figure 3d. If the U^{6+}-species would be coordinatively unsaturated (like the Cu^{++} species in HKUST-1),[19a] we would expect a $U^{\delta+}$-CO vibrational band in the higher wavenumber region with a blue-shift compared to the CO gas phase value.[20] After prolonged exposure, only a CO vibrational band at 2140 cm^{-1} was observed, which is characteristic for CO ice.[21] When the KIT-U-1 was activated by pre heating to 450 K for 20 min in the UHV system, as shown in Figure S7, a weak signal at 2179 cm^{-1} was observed. We

assign this peak to a $U^{\delta+}$-CO species and explain this observation by temperature-induced formation of defects inside the KIT-U-1.[19a,21,22] The absence of adsorption sites for CO on the U-ions is fully consistent with the structural model shown in Figure S6. The MOF thin films were also investigated by X-ray photoelectron spectroscopy (XPS). The U 4f doublet appeared at 381.9 (U $4f_{7/2}$) and 392.7 eV (U $4f_{5/2}$), which are assigned to U^{6+} species. The characteristic satellites of U $4f_{7/2}$ and U $4f_{5/2}$ were observed as well. Thus, the uranium atom in the KIT-U-1 thin film was demonstrated as a hexavalent state. A substantial amount of reduction during the LbL assembly can thus be ruled out.

The experimental characterization of the crystal structure of KIT-U-1 was complemented by DFT calculations, which provided a detailed understanding of the local coordination environment of the uranyl units and revealed their arrangement into 2D layers, and the preferred stacking order of the layers. Figure 4a and 4b show the DFT-optimized structure whose simulated PXRD exhibits the best agreement with the experimental in-plane and out-of-plane patterns (Figure 1b). As one can see, KIT-U-1 has a well-defined layered structure, and in each layer the UO_2^{2+} units are bridged via fully deprotonated BTC^{3-} linkers. Each UO_2^{2+} unit is coordinated via three carboxylate moieties to three different BTC^{3-} ligands and each BTC^{3-} ligand chelates three UO_2^{2+} units. Thus, a 2D graphene-like net is formed, in which alternating UO_2^{2+} and BTC^{3-} ions make up the hexagons, and each of the so-formed hexagonal pores accommodates one $[H\text{-}TEA]^+$ cation that keeps the charge neutrality of the layer (Figure 4c). Note that in the unit cell representing the crystal structure, there is a 1:1:1 ratio between UO_2^{2+}, BTC^{3-}, and $[H\text{-}TEA]^+$. Combined with the LC-ESI-MS characterization of the dissolved thin film (Figure 2d), this indicates that the $[H\text{-}TEA]^+$ cations are an important component in the structure of KIT-U-1. The charged $[H\text{-}TEA]^+$ cations are essential for charge balancing

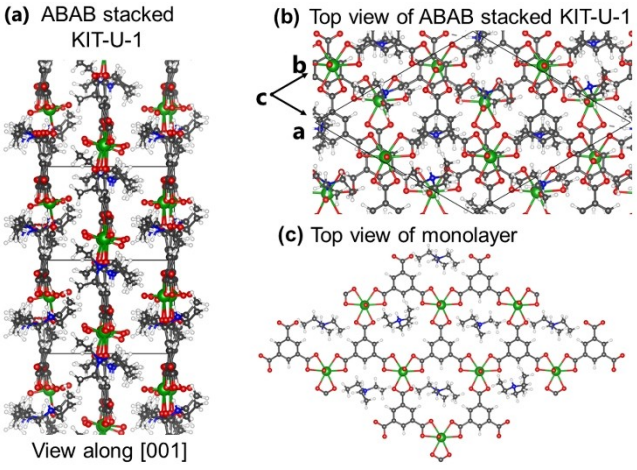

Figure 4. Atomistic representation of KIT-U-1 in ABAB stacking along (a) [001] and (b) [100] direction. The DFT-optimized lattice vectors of the hexagonal unit cell, indicated by the quadrilaterals, are $a=b=17.155$ Å, $c=11.661$ Å ; (c) Top view of a KIT-U-1 monolayer. Color code: U green, O red, N blue, C grey, H white.

of the uranyl-based structure during the LbL assembly process. In the following we describe DFT calculations of the KIT-U-1 to confirm these experimental results.

Within each $[UO_2(BTC)_3]^-$ secondary building unit, the DFT calculated bond lengths between the uranium ion and the six equatorial carboxylic oxygen atoms, $U–O_{eq}$, vary in the range from 2.46 to 2.58 Å, and those between uranium and the axial uranyl oxygens, $U–O_{ax}$, are in the range from 1.796 to 1.807 Å. This clearly shows the sixfold and rather symmetric coordination environment of the uranyl ions. These observations are fully consistent with the experimental Raman and IRRAS characterization. As shown in Figure 4b and 4c, the graphene-like layers are stacked in ABAB sequence, such that the benzene rings from the second layer are located on top of the hexagonal pores of the first layer. In the so-formed staggered structure, the UO_2^{2+}, BTC^{3-} and $[H\text{-}TEA]^+$ components of the middle layer are overlaid by the $[H\text{-}TEA]^+$, UO_2^{2+}, and BTC^{3-} components of the top and bottom layers respectively (Figure 4a). The calculated U···U next-neighbor distances are of the order of 9.94 ± 0.05 Å within each layer and vary from 7.43 Å to 8.54 Å between adjacent layers. These values are much larger than the U···U distances typical for crystalline U(VI) materials with cation-cation interactions (CCIs)[23] hence, we can exclude the existence of CCIs between the UO_2^{2+} ions in KIT-U-1. This was confirmed by the experimental Raman spectrum of the KIT-U-1 thin film (see Figure 3a and related discussion). Finally, our calculations indicate that the guest cations in the KIT-U-1 structure are important for compensating the charge of the $[UO_2(BTC)_3]^-$ anionic SBUs, and they control the distance between the adjacent 2D layers. If we replace the $[H\text{-}TEA]^+$ cations with some less bulky cations, such as NH^{4+} in Figure S5, the size of the optimized unit cell in the direction between the layers decreases from 11.66 Å to 8.93 Å. (see Supporting Information for details). However, $[UO_2(BTC)_3]^-$ with the $[H\text{-}TEA]^+$ cations as guest cations is the only stable structure formed during LbL synthesis.

The photoluminescent nature of the KIT-U-1 thin film was first investigated at 297 K and 77 K. Under excitation with 315 nm light, the KIT-U-1 thin film on quartz glass exhibited characteristic emission peaks in the visible light range, as shown in Figure 5a. At 77 K, the emission peaks were located at 482, 503, 524, 549, and 575 nm, which are related to S_{10} to S_{0v} ($v=0$–4).[10,24] The transition from S_{10} to S_{01} at 503 nm exhibited the highest intensity. The energy difference between the bands of S_{10}-to-S_{00} and S_{10}-to-S_{01} transitions was recorded as 869 cm^{-1}, which corresponds well with the band observed in the Raman spectra, as depicted in Figure 3a. When the KIT-U-1 thin film was heated to 297 K, a different emission spectrum was observed with six emission peaks located at 464, 482, 503, 525, 549, and 576 nm.

At 297 K the emission spectrum exhibits an additional peak at 464 nm compared to that recorded at 77 K and the peak at 483 nm exhibits the highest intensity, in contrast to low temperatures, where the emission at 503 nm is the strongest. Although the emission at 464 nm has been observed before in a few uranium-based MOFs, in the

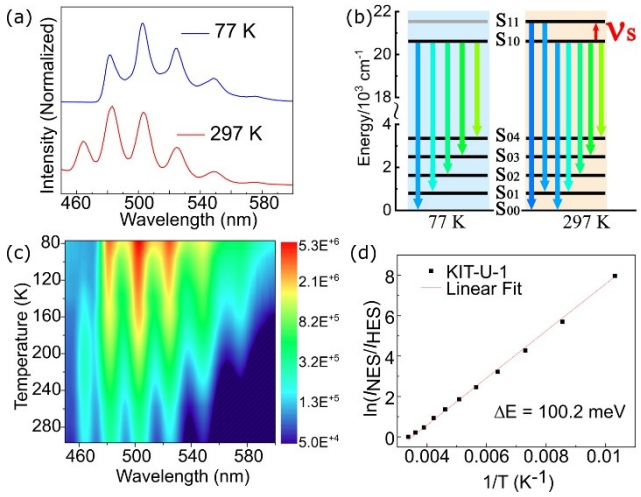

Figure 5. (a) Emission spectra of KIT-U-1 thin film at 77 K (blue) and 297 K (red); (b) schematic illustration of the emission process in KIT-U-1 thin film at 77 K and 297 K; (c) Two-dimensional map of the temperature-dependent photoluminescent spectra of KIT-U-1 thin film; (d) Plotting of the natural logarithm of photoluminescent intensity ratio between the normal excited state and the first hot excited state against reciprocal temperature for KIT-U-1, $R^2 = 0.998$.

previous work this feature has not been analyzed in more detail, presumably due to the weakness of the peak for the previously synthesized U-MOFs.[6b,c]

The occurrence of such a "hot band"[10,25] can be explained by the Jablonski diagram shown in Figure 5b. At low temperatures (77 K), the excited state S_{10} (20746 cm^{-1}) is the only state which is populated upon irradiation with UV light. From there, electronic transitions into the S_{0v} (v = 0–4) levels take place, leading to five emission lines.[10,26] We explain the additional emission peak at 464 nm occurring at higher temperatures by electronic transitions with the S_{11} state (21551 cm^{-1}) as the initial state and the S_{00} state as the final state.[10,25] Again, S_{0v} (v = 0–4) are the final states. Since the S_{11} state cannot be populated directly by the incident UV-light (as evident from the data recorded at 77 K) we conclude that it is populated by excitation of electrons in the S_{10} state via absorption of phonon from the MOF lattice. In fact, the O–U–O symmetric vibration (Vs) at 820 cm^{-1} (see the Raman data in Figure 3a) has the right energy for such a transition. The KIT-U-1 thin films with various thickness exhibited similar temperature-dependent photoluminescent properties, as shown in Figure S9, which indicated the electron-phonon coupling is intrinsic to the crystalline structure. Meanwhile, the overlap of emissions from S_{11}-to-S_{0n} and S_{10}-to-$S_{0(n-1)}$ ($n = 1$–4) induced the unusual intensity change in the peaks at 483, 503, 525, 549, and 576 nm.

This apparent importance of electron-phonon coupling has not yet been observed for MOFs and other framework materials and suggests that further research is needed for conductive MOFs and their optoelectronic and electronic properties.

In KIT-U-1, the uranyl units are highly symmetric coordinated by the six oxygen atoms from the BTC linker in the equatorial plane.[25b,27] To our knowledge, the KIT-U-1 thin film presented here exhibited the largest ratio (> 40 %) of the hot band to the main emission band at 503 nm (S_{10}–S_{01}) among all uranyl-based MOFs.[6,28]

To further investigate the temperature-dependent "hot-band" emission, the photoluminescent properties of KIT-U-1 were also measured beyond room temperature, as shown in Figure 6. Surprisingly, in addition to the first "hot-band" emission at 464 nm (HB1), a second "hot-band" emission was observed at 448 nm (HB2), which is related to S_{12}-to-S_{00} transition. The S_{12} state (22321 cm^{-1}) is populated by excitation of electrons in the S_{11} state via the electron-phonon coupling. As far as we know, this is the first observation of a second hot band among all uranium-based materials and rare-earth MOFs.

The coupling strength of the "Hot-band" emission at 464 nm in KIT-U-1 was determined from the experimental data by calculating the "Huang–Rhys" factor (S) by measuring the full-width at half-maximum (FWHM) of the emission at 464 nm in KIT-U-1 thin film from 100 to 400 K and fitting the data with the following equation:[29]

$$FWHM = \sqrt{8ln2}\hbar\omega\sqrt{Scoth\frac{\hbar\omega}{2k_BT}}$$

Here $\hbar\omega$ denotes the phonon energy and k_B is the Boltzmann constant. The obtained S is 3.16, which reveals that this soft MOF thin film has a quite strong coupling strength.[30]

A two-dimensional map of the temperature-dependent photoluminescent spectra of KIT-U-1 thin film was recorded from 77 K to room temperature for visualizing the temperature-dependent emission, as shown in Figure 5c.

The overlap of the emissions from the "hot" state S_{11} and the normal excited state S_{10} can be separated using a

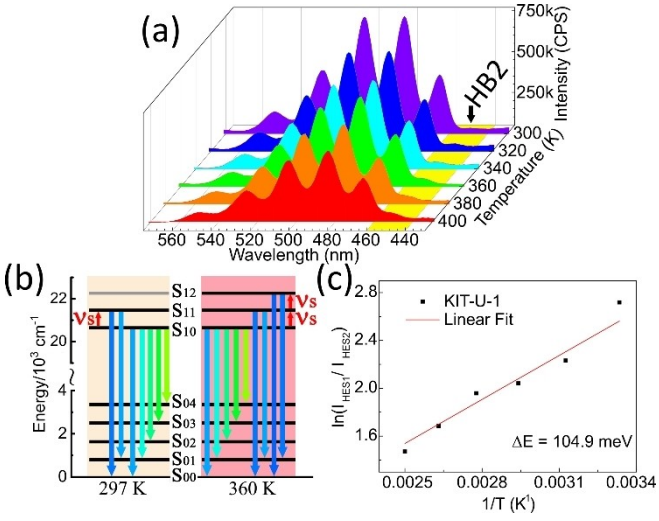

Figure 6. (a) Emission spectra of KIT-U-1 thin film from 300 K to 400 K; (b) schematic illustration of the emission process in KIT-U-1 thin film at 297 K and 360 K; (c) Plotting of the natural logarithm of photoluminescent intensity ratio between the first hot excited state (HB1) and the second hot excited state (HB2) against reciprocal temperature for KIT-U-1, $R^2 = 0.950$.

fitting procedure as shown in Figure S10. The intensities of the different transitions from the hot S_{11} state and the S_{10} state can be given as follows:[31]

$$\frac{I_{NES}}{I_{HES}} = \frac{N_{NES}}{N_{HES}} = e^{(\varepsilon_{HES}-\varepsilon_{NES})/kT} = e^{\Delta E/kT}$$

where I_{NES} and N_{NES} are the intensity and the population of the normal excited S_{10} state; I_{HES} and N_{HES} are the intensity and the population of the hot excited S_{11} state; ΔE is the energy gap between hot excited S_{11} state and normal excited S_{10} state.

As shown in Figure 5d, a Boltzmann-type analysis of this feature reveals an effective activation energy of 100.2 meV, closely approximating the energy gap between the S_{10} and the S_{11} states. The same Boltzmann-type analysis was also applied to the HB2 peak at 448 nm. The obtained effective activation energy of HB2 is 104.9 meV, which is also close to the observed energy gap between the S_{11} and the S_{12} states. This analysis of the temperature dependence thus confirms the assignment of the hot band to luminescence from two phonon-associated excited states.[32] To our knowledge, this marks the first time that the temperature-dependent behavior of a distinct hot band in luminescence has been comprehensively analyzed, enabling a clear identification of the associated phonon.

Theoretical justification for the assignment of the hot bands seen in our experiments was provided by performing ab-initio electronic structure calculations where the coupling of excited states to lattice phonons is considered in the framework of time-dependent DFT (TDDFT) calculations. A simplified model sufficient to reproduce the experimental findings was constructed by choosing a highly symmetric $[UO_2–(BC)_3]^{-1}$ cluster, where BC denotes a benzene carboxylic acid (Figure S13). Vibronic structure tracking analysis for the excited state was conducted on the optimized structure at DFT theory level. The dominant vibrational mode for the coupling to the excited state is the symmetric stretching of UO_2^{2+} with a frequency of 848 cm^{-1} in the ideal $[UO_2–(BC)_3]^{-1}$ model. According to the calculations, this coupling yields hot bands at 446 and 464 nm. These predicted values agree well with experimental ones, 448 nm and 464 nm (Figure S14). For more details on these calculations see the Supporting Information.

The implications of these findings extend beyond gaining fundamental insight and allow for a direct application. As shown in Figure 7, the U-based MOFs provide a platform for fabricating single-compound optical thermometers for a wide temperature range (from 77 K to 400 K). The key performance indicator of such a device is the thermometric parameter Δ. The thermal sensitivity S_r was calculated from the thermometric parameter Δ and the sensitivity S_r indicated the relative change of the thermometric parameter Δ in per degree of temperature change. The thermometric parameter Δ and the thermal sensitivity S_r are defined by:[11a,33]

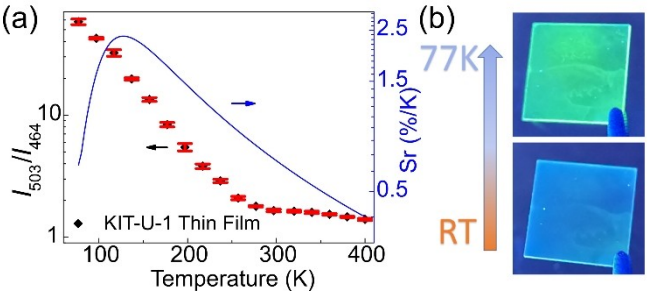

Figure 7. (a) Evolution with temperature of the thermometric parameter △ (black), error bars (red) in Figures show the standard error, and thermal sensitivity S_r (blue) of the KIT-U-1 thin film; (b) Optical photographs of KIT-U-1 thin film at 77 K (top) and room temperature (bottom).

$$\Delta = \frac{I_{503}}{I_{464}}$$

$$S_r = \frac{1}{\Delta}\left|\frac{\partial \Delta}{\partial T}\right|$$

where I_{503} and I_{464} are the intensities of the emission at 503 nm and 464 nm.

The KIT-U-1 thin film exhibited a sensitivity exceeding 1 %/K over the temperature range of 90 K to 260 K, as well as a sensitivity surpassing 0.5 %/K from 77 K to 360 K. As shown in Figure S12, the thermometric parameters showed no substantial variation during subsequent heating/cooling cycles. This single-metal ratiometric thermometer, simple to produce, showed significant sensitivity over a wide sensing range. This is in contrast to normal lanthanides-doped optical thermometers, which require at least two distinct metal ions,[34] making the new KIT-U-1 thermometer more efficient.

Conclusion

In summary, we have successfully fabricated continuous, crystalline, and oriented KIT-U-1 MOF thin films showing a pair of hot bands in photoluminescence. The 2D structure of KIT-U-1 was determined using a combination of DFT simulations and experimental results. The uranyl units in this KIT-U-1 structure exhibit a highly symmetrical coordination, yielding two unusual thermal-activated emission bands (“hot-bands”). These luminescence features are a direct result of strong electron-phonon coupling, as confirmed by ab-initio electronic structure calculations explicitly treating the coupling of the electronic excited states to lattice phonons. The strong and characteristic “hot-band” emission phenomenon in the KIT-U-1 thin films allowed to fabricate, in a straightforward fashion, a sensitive, single-component thermometer with optical readout of exceptional thermal sensitivity. In the future, KIT-U-1 and related actinide-based MOF thin films are expected to find more applications in numerous other fields, including biomedical imaging, nuclear science, or protective coatings.

Supporting Information

The authors have cited additional references within the Supporting Information.[35–43]

Acknowledgements

The authors also would like to thank Peter G. Weidler and Stefan Heissler for their technical assistance on the XRD measurements and Raman measurements. The Center for Information Services and High Performance Computing (ZIH) at TU Dresden and the Paderborn Center for Parallel Computing (PC2) are acknowledged for computational resources. Open Access funding enabled and organized by Projekt DEAL.

Conflict of Interest

The authors declare no conflict of interest.

Data Availability Statement

The data that support the findings of this study are available from the corresponding author upon reasonable request.

Keywords: Uranium Metal–Organic Frameworks · Thin Film · DFT Calculation · Electron-Phonon Coupling · Single-Metal Ratiometric Thermometer

[1] a) C. Zhang, W. Li, L. Li, *Angew. Chem. Int. Ed.* **2021**, *60*, 7488–7501; b) Q. Lv, X. Wang, L. Liao, *Adv. Funct. Mater.* **2022**, *32*, 2202364.
[2] C. Ng, L. Wesemann, E. Panchenko, J. Song, T. J. Davis, A. Roberts, D. E. Gómez, *Adv. Opt. Mater.* **2019**, *7*, 1801660.
[3] M. Gutiérrez, Y. Zhang, J.-C. Tan, *Chem. Rev.* **2022**, *122*, 10438–10483.
[4] L. Heinke, C. Wöll, *Adv. Mater.* **2019**, *31*, 1806324.
[5] R. Medishetty, J. K. Zaręba, D. Mayer, M. Samoć, R. A. Fischer, *Chem. Soc. Rev.* **2017**, *46*, 4976–5004.
[6] a) P. Thuéry, J. Harrowfield, *Inorg. Chem.* **2016**, *55*, 6799–6816; b) Y. Zhang, I. Karatchevtseva, M. Bhadbhade, T. T. Tran, I. Aharonovich, D. J. Fanna, N. D. Shepherd, K. Lu, F. Li, G. R. Lumpkin, *J. Solid State Chem.* **2016**, *234*, 22–28; c) Y. Wang, X. Yin, W. Liu, J. Xie, J. Chen, M. A. Silver, D. Sheng, L. Chen, J. Diwu, N. Liu, Z. Chai, T. E. Albrecht-Schmitt, S. Wang, *Angew. Chem. Int. Ed.* **2018**, *57*, 7883–7887.
[7] S. Begum, Z. Hassan, S. Bräse, C. Wöll, M. Tsotsalas, *Acc. Chem. Res.* **2019**, *52*, 1598–1610.
[8] a) K. C. Park, P. Kittikhunnatham, J. Lim, G. C. Thaggard, Y. Liu, C. R. Martin, G. A. Leith, D. J. Toler, A. T. Ta, N. Birkner, I. Lehman-Andino, A. Hernandez-Jimenez, G. Morrison, J. W. Amoroso, H.-C. zur Loye, D. P. DiPrete, M. D. Smith, K. S. Brinkman, S. R. Phillpot, N. B. Shustova, *Angew. Chem. Int. Ed.* **2023**, *62*, e202216349; b) Y. Zhang, X. Wang, K. Xu, F. Zhai, J. Shu, Y. Tao, J. Wang, L. Jiang, L. Yang, Y. Wang, W. Liu, J. Su, Z. Chai, S. Wang, *J. Am. Chem. Soc.* **2023**, *145*, 13161–13168; c) C. R. Martin, G. A. Leith, P. Kittikhunnatham, K. C. Park, O. A. Ejegbavwo, A. Mathur, C. R. Callahan, S. L. Desmond, M. R. Keener, F. Ahmed, *Angew. Chem. Int. Ed.* **2021**, *60*, 8072–8080.
[9] a) A. Kovacs, R. J. Konings, J. K. Gibson, I. Infante, L. Gagliardi, *Chem. Rev.* **2015**, *115*, 1725–1759; b) T. Zheng, Y. Gao, D. Gui, L. Chen, D. Sheng, J. Diwu, Z. Chai, T. E. Albrecht-Schmitt, S. Wang, *Dalton Trans.* **2016**, *45*, 9031–9035.
[10] J. Su, K. Zhang, W. E. Schwarz, J. Li, *Inorg. Chem.* **2011**, *50*, 2082–2093.
[11] a) D.-H. Chen, R. Haldar, C. Wöll, *ACS Appl. Mater. Interfaces* **2023**, *15*, 19665–19671; b) B. Yan, *Inorg. Chem. Front.* **2021**, *8*, 201–233.
[12] D.-H. Chen, H. Gliemann, C. Wöll, *Chem. Phys. Rev.* **2023**, *4*, 011305.
[13] C. Volkringer, I. Mihalcea, J.-F. Vigier, A. Beaurain, M. Visseaux, T. Loiseau, *Inorg. Chem.* **2011**, *50*, 11865–11867.
[14] a) P. Li, N. A. Vermeulen, X. Gong, C. D. Malliakas, J. F. Stoddart, J. T. Hupp, O. K. Farha, *Angew. Chem. Int. Ed.* **2016**, *55*, 10358–10362; b) R. Christoffels, C. Breitenbach, J. P. Weber, L. Körtgen, C. Tobeck, M. Wilhelm, S. Mathur, J.-M. Neudörfl, M. S. Z. Farid, M. Maslo, E. Strub, U. Ruschewitz, *Cryst. Growth Des.* **2021**, *22*, 681–692.
[15] V. Blatov, *Struct. Chem.* **2012**, *23*, 955–963.
[16] S. Friedländer, J. Liu, M. Addicoat, P. Petkov, N. Vankova, R. Rüger, A. Kuc, W. Guo, W. Zhou, B. Lukose, Z. Wang, P. G. Weidler, A. Pöppl, M. Ziese, T. Heine, C. Wöll, *Angew. Chem. Int. Ed.* **2016**, *55*, 12683–12687.
[17] P. M. Cantos, L. J. Jouffret, R. E. Wilson, P. C. Burns, C. L. Cahill, *Inorg. Chem.* **2013**, *52*, 9487–9495.
[18] a) M. A. Czarnecki, Y. Morisawa, Y. Futami, Y. Ozaki, *Chem. Rev.* **2015**, *115*, 9707–9744; b) D.-H. Chen, R. Haldar, B. L. Neumeier, Z. Fu, C. Feldmann, C. Wöll, E. Redel, *Adv. Funct. Mater.* **2019**, *29*, 1903086.
[19] a) W. Wang, D. I. Sharapa, A. Chandresh, A. Nefedov, S. Heißler, L. Heinke, F. Studt, Y. Wang, C. Wöll, *Angew. Chem. Int. Ed.* **2020**, *59*, 10514–10518; b) J. Song, X. Yu, A. Nefedov, P. Weidler, S. Grosjean, S. Bräse, Y. Wang, C. Wöll, *Angew. Chem. Int. Ed.* **2023**, e202306155.
[20] Y. Wang, C. Wöll, *Chem. Soc. Rev.* **2017**, *46*, 1875–1932.
[21] J. Wang, W. Wang, Z. Fan, S. Chen, A. Nefedov, S. Heißler, R. A. Fischer, C. Wöll, Y. Wang, *J. Phys. Chem. C* **2021**, *125*, 593–601.
[22] Z. Fang, B. Bueken, D. E. De Vos, R. A. Fischer, *Angew. Chem. Int. Ed.* **2015**, *54*, 7234–7254.
[23] V. Serezhkin, G. Sidorenko, D. Pushkin, L. Serezhkina, *Radiochemistry* **2014**, *56*, 115–133.
[24] A. Brachmann, G. Geipel, G. Bernhard, H. Nitsche, *Radiochim. Acta* **2002**, *90*, 147–153.
[25] a) H. Oher, G. Ferru, L. Couston, L. Berthon, D. Guillaumont, F. Réal, T. Vercouter, V. Vallet, *Inorg. Chem.* **2021**, *61*, 890–901; b) B. Drobot, A. Bauer, R. Steudtner, S. Tsushima, F. Bok, M. Patzschke, J. Raff, V. Brendler, *Anal. Chem.* **2016**, *88*, 3548–3555.
[26] E. Rabinowitch, R. L. Belford, *Spectroscopy and Photochemistry of Uranyl Compounds*, The MacMillan Company, New York **1964**.
[27] T. Haubitz, B. Drobot, S. Tsushima, R. Steudtner, T. Stumpf, M. U. Kumke, *J. Phys. Chem. A* **2021**, *125*, 4380–4389.
[28] J. Xie, Y. Wang, M. A. Silver, W. Liu, T. Duan, X. Yin, L. Chen, J. Diwu, Z. Chai, S. Wang, *Inorg. Chem.* **2018**, *57*, 575–582.
[29] a) Y. Zhuo, A. Mansouri Tehrani, A. O. Oliynyk, A. C. Duke, J. Brgoch, *Nat. Commun.* **2018**, *9*, 4377; b) K. Huang, A. Rhys, *Proc. R. Soc. Lond. Ser. Math. Phys. Sci.* **1950**, *204*, 406–423.
[30] a) G. Liu, M. Jensen, *Chem. Phys. Lett.* **2010**, *499*, 178–181; b) G. Liu, N. P. Deifel, C. L. Cahill, V. V. Zhurov, A. A. Pinkerton, *J. Phys. Chem. A* **2012**, *116*, 855–864; c) G. Liu, S.

Wang, T. E. Albrecht-Schmitt, M. P. Wilkerson, *J. Phys. Chem. A* **2012**, *116*, 8297–8302.
[31] a) F. Qin, H. Zhao, W. Cai, Z. Zhang, W. Cao, *Appl. Phys. Lett.* **2016**, *108*, 241907; b) M. Back, J. Ueda, M. G. Brik, S. Tanabe, *ACS Appl. Mater. Interfaces* **2020**, *12*, 38325–38332.
[32] A. A. Ansari, A. K. Parchur, M. Nazeeruddin, M. M. Tavakoli, *Coord. Chem. Rev.* **2021**, *444*, 214040.
[33] Z. Wang, D. Ananias, A. Carné-Sánchez, C. D. Brites, I. Imaz, D. Maspoch, J. Rocha, L. D. Carlos, *Adv. Funct. Mater.* **2015**, *25*, 2824–2830.
[34] J. Rocha, C. D. Brites, L. D. Carlos, *Chem. Eur. J.* **2016**, *22*, 14782–14795.
[35] N. Zhang, Y.-H. Xing, F.-Y. Bai, *Inorg. Chem.* **2019**, *58*, 6866–6876.
[36] a) Y. Wang, Z. Liu, Y. Li, Z. Bai, W. Liu, Y. Wang, X. Xu, C. Xiao, D. Sheng, J. Diwu, J. Su, Z. Chai, T. E. Albrecht-Schmitt, S. Wang, *J. Am. Chem. Soc.* **2015**, *137*, 6144–6147; b) X.-L. Zhang, K.-Q. Hu, L. Mei, Y.-B. Zhao, Y.-T. Wang, Z.-F. Chai, W.-Q. Shi, *Inorg. Chem.* **2018**, *57*, 4492–4501; c) J. Su, J. Chen, *Lanthan. Met.-Org. Framew.* **2015**, *163*, 265–295.
[37] T. D. Kühne, M. Iannuzzi, M. Del Ben, V. V. Rybkin, P. Seewald, F. Stein, T. Laino, R. Z. Khaliullin, O. Schütt, F. Schiffmann, *J. Chem. Phys.* **2020**, *152*, 194103.
[38] J. P. Perdew, K. Burke, M. Ernzerhof, *Phys. Rev. Lett.* **1996**, *77*, 3865.
[39] a) J. VandeVondele, J. Hutter, *J. Chem. Phys.* **2007**, *127*, 114105; b) S. Goedecker, M. Teter, J. Hutter, *Phys. Rev. B* **1996**, *54*, 1703.
[40] J.-B. Lu, D. C. Cantu, C.-Q. Xu, M.-T. Nguyen, H.-S. Hu, V.-A. Glezakou, R. Rousseau, J. Li, *J. Chem. Theory Comput.* **2021**, *17*, 3360–3371.
[41] a) S. Grimme, J. Antony, S. Ehrlich, H. Krieg, *J. Chem. Phys.* **2010**, *132*, 154104; b) S. Grimme, S. Ehrlich, L. Goerigk, *J. Comput. Chem.* **2011**, *32*, 1456–1465.
[42] G. t Te Velde, F. M. Bickelhaupt, E. J. Baerends, C. Fonseca Guerra, S. J. van Gisbergen, J. G. Snijders, T. Ziegler, *J. Comput. Chem.* **2001**, *22*, 931–967.
[43] K. Momma, F. Izumi, *J. Appl. Crystallogr.* **2011**, *44*, 1272–1276.

Manuscript received: December 4, 2023
Accepted manuscript online: December 28, 2023
Version of record online: ■■, ■■

Research Articles

Metal-Organic Frameworks

D.-H. Chen,* N. Vankova, G. Jha, X. Yu, Y. Wang, L. Lin, F. Kirschhöfer, R. Greifenstein, E. Redel, T. Heine, C. Wöll* _____ e202318559

Ultrastrong Electron-Phonon Coupling in Uranium-Organic Frameworks Leading to Inverse Luminescence Temperature Dependence

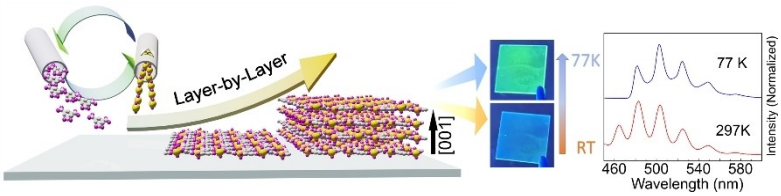

A consistent, crystalline, and oriented uranium-based MOF thin film was devised by using a layer-by-layer technique. The materials exhibited a noticeable phonon-assisted temperature-dependent photoluminescence and presented two unusual thermal-activated emission bands ("hot-band"). A single-metal ratiometric optical thermometer was designed relying on this uranium-based MOF thin films and it exhibited exceptional thermal sensitivity.